IEEE Access
Multidisciplinary ⋮ Rapid Review ⋮ Open Access Journal

Received November 18, 2021, accepted December 1, 2021, date of publication December 13, 2021,
date of current version January 10, 2022.

Digital Object Identifier 10.1109/ACCESS.2021.3134951

Outage Analysis of Relay-Based Dual-Hop Hybrid FSO-mmWave Systems

SEZER C. TOKGOZ[1,2], (Graduate Student Member, IEEE), SAUD ALTHUNIBAT[3], (Senior Member, IEEE), SCOTT L. MILLER[1], (Fellow, IEEE), AND KHALID A. QARAQE[2], (Senior Member, IEEE)

[1]Department of Electrical and Computer Engineering, Texas A&M University, College Station, TX 77843, USA
[2]Department of Electrical and Computer Engineering, Texas A&M University at Qatar, Doha, Qatar
[3]Department of Communications Engineering, Al-Hussein Bin Talal University, Ma'an 71111, Jordan

Corresponding author: Sezer C. Tokgoz (sezer_can.tokgoz@tamu.edu)

This work was supported in part by the Ooredoo Research Sponsorship, and in part by the Qatar National Research Fund (a member of the Qatar Foundation) under Grant NPRP12S-0225-190152. The statements made herein are solely the responsibility of the author[s].

ABSTRACT Bearing in mind the high data rate and volume requirements of 5G and beyond networks, millimeter wave (mmWave) systems can be utilized with the assistance of free-space optical (FSO) systems since both technologies exhibit distinctive behaviors under different weather conditions. Therefore, in this study, we investigate a relay-based dual-hop hybrid FSO-mmWave systems from an outage performance point of view, where the communication in each hop is established on both FSO and mmWave links simultaneously. Specifically, Nakagami-m distribution is used for mmWave fading channels, while gamma-gamma distribution is assumed for FSO turbulence channels. Two well-known amplify-and-forward (AF) relaying schemes are examined during data transmission, in which the power amplification operation is based on partial and full channel state information of the system, namely, fixed-gain and variable-gain AF relaying methods. The effects of fundamental system variables on the outage analysis of the relay-based hybrid transmissions are investigated by obtaining exact closed-form derivations of the outage probability and effective throughput. Based upon the results, it is shown that the proposed closed-form expressions are in good match with the Monte-Carlo simulations.

INDEX TERMS Dual-hop relay, free space optical, hybrid FSO-mmWave systems, millimeter wave, outage performance.

I. INTRODUCTION

The constant increase of wireless data rate and volume of 5G and beyond networks push academia and industry to research on higher frequency spectrum. Based on the current studies and reports, it is predicted that the average data volume will be at least thousand times higher than 4G requirements [1]. Free-space optical (FSO) systems as an optical wireless communications are proposed as an optimistic solution for high speed wireless systems due to its natural benefits like robustness to interference, low power consumption, and as well as higher security level than traditional radio frequency (RF) transmissions [2]. However, an FSO link is highly dependent on line-of-sight (LOS) adjustments and is dramatically influenced by different turbulence circumstances including temperature, wind strength, and foggy atmosphere [3], [4]. As an alternative solution, researchers show that millimeter waves (*mm*Wave) bands also support multi-gigabit wireless data transmissions with very low latency [5]. Additionally, the environment conditions that dramatically decrease the reliability of FSO systems have trivial effects on *mm*Wave transmissions. However, *mm*Wave bands are heavily affected by rainy conditions and oxygen absorbance, and considered as more susceptible to security assaults [6], where FSO links have very high strength. The complementary behaviors of both transmission technology against different conditions pave the way for parallel employment of *mm*Wave and FSO links to satisfy quality of service requirements of 5G and beyond networks [7]. Furthermore, wireless data rates supported by each transmission are compatible to each other, which enable the parallel employment of both links to increase spectral efficiency or transmit diversity [8]–[10].

The associate editor coordinating the review of this manuscript and approving it for publication was Olutayo O. Oyerinde.

By other means, multi-hop relaying schemes are widely used as energy efficient techniques to increase the system reliability, coverage area, and capacity [11]. Therefore, considering high demands/requirements of 5G and beyond era, relay-based methods have been extensively employed to improve quality of services. In such systems, the message signal is transmitted over either FSO or RF link from source to relay node which is then forwards this message over other link to the destination node.

A. RELATED WORKS

In the light of motivations explained above, related studies has been significantly boosted in the open literature during the last few years. For example, mixed dual- and multi-hop relaying methods are extensively investigated in [12]–[20] for FSO and RF systems considering both fixed- and variable-gain amplift-and-forward (AF) relaying schemes taking several fundamental physical layer parameters into account under various scenarios and configurations. The authors in [21]–[24] examine a partial AF relay selection is assumed for mixed system, in which the channel state information is considered as outdated. Further, a detailed performance analysis of mixed RF-FSO systems is examined in [25]–[28] considering cooperative transmissions, in which the impact of co-channel interference is assumed at each hop, threshold-based selective switching schemes, moment generating function, amount of fading and higher order moments are also taken into account. On the other hand, in the works [29]–[34], dual-hop mixed FSO and RF wireless communication systems are studied for both fixed- and variable-gain AF relaying methods considering single eavesdropper which only wire-taps on RF links. The authors then investigated the secrecy performance of the system by using the analytical derivations of the secrecy outage probability and capacity metrics.

B. MOTIVATION

In the open literature, majority of the studies discussed above examines relay-based dual-hop mixed FSO and RF systems under various configurations and scenarios, in which either RF or FSO transmission is employed in one of the hops. However, as previously explained, the service quality of relay-based dual-hop mixed systems are significantly decreased under particular atmospheric environments. To eliminate this issue, a promising remedy is to utilize both FSO and RF systems with parallel/simultaneous transmissions since both technology has complementary characteristics with respect to distinct environments. Additionally, low latency, high reliability, and high throughput are needed to satisfy the demanding requirements of 5G and beyond era, in comparison with 4G, in which the traditional RF back-haul networks are generally limited by low capacity. Therefore, single hop hybrid FSO-RF parallel transmissions are examined in [35]–[42] under various scenarios. Thus, with these motivations, in this study, dual-hop relaying techniques is combined with hybrid FSO-RF systems to extend the communication distance, and to satisfy the reliability, low latency and high capacity requirements of 5G and beyond era. The main difference between this study and the other studies is the use of both FSO and RF links in each hop of the transmission. In particular, we examine two well-known AF relaying schemes during data transmission, in which the power amplification operation is made by using either partial or full system's channel state information, namely, fixed-gain and variable-gain AF relaying methods, respectively, where the communication in each hop is carried over both RF and FSO links simultaneously.

C. CONTRIBUTIONS

The major contributions of this work can be enumerated as follows:

1) Although hybrid FSO-RF transmissions are very optimistic remedies for back-haul networks of 5G and beyond era, outage analysis of dual-hop hybrid FSO-RF systems have not yet been addressed in open literature to the best of authors' knowledge. Therefore, we investigate a hybrid FSO-RF system with relaying methods, where the communication in each hop is established through both FSO and RF systems simultaneously.
2) To make more insightful findings about relay-based dual-hop hybrid FSO-RF systems, we take various fundamental physical layer parameters into account and present detailed discussions and conclusions.
3) To provide the main impacts for practical scenarios of interest, FSO links are subject to Gamma-Gamma distributed atmospheric turbulence including two different detection techniques, i.e, intensity-modulation/direct-detection (IM/DD) and heterodyne detection, in the presence of pointing errors, while RF link are considered as Nakagami-m distributed fading channels.
4) Novel exact closed-form derivations are provided for the metrics of outage probability and effective throughout, considering fixed- and variable-gain AF relaying methods. Additionally, asymptotic derivation are also presented to illustrate system performance in high average signal-to-noise ratio (SNR) regions.
5) To illustrate the correctness of the proposed analytical derivations, Monte-Carlo based simulation results are given along with related theoretical findings including various fundamental physical layer parameters.

D. PAPER ORGANIZATION

The organization of this manuscript can be summarized as: System model of hybrid FSO-*mm*Wave communications is described in Section II including the channel characteristics, and definitions of signal-to-noise ratios. Section III presents the outage analysis of dual-hop hybrid FSO-*mm*Wave system fixed- and variable-gain AF relaying schemes. The finding are given in Section IV along with a detailed discussions. Finally, the manuscript is concluded in Section V.

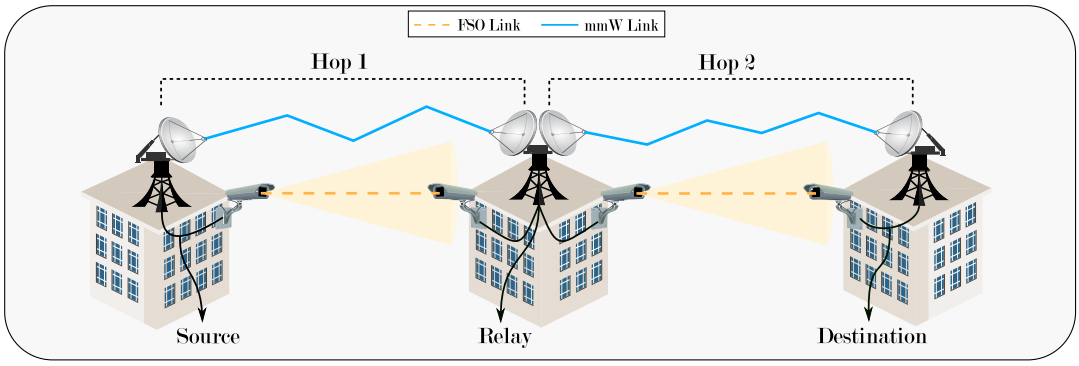

FIGURE 1. System block model of relay-based dual hop hybrid FSO-*mm*Wave communications.

II. SYSTEM MODEL

A scenario is taken into consideration in which dual-hop relaying systems are considered for data transmissions. The source wants to send an information signal to the destination by the use of a relay, as illustrated in Fig. 1. The communication in first hop (from source to relay) and second hop (from relay to destination) are established over two parallel links, called as, FSO and RF links. Therefore, it is presumed that transmitter nodes (source and relay) have a single transmitting antenna and laser, while receiver nodes (relay and destination) have a single receiving antenna and photodetector. Information bits to be transmitted are divided into $\log_2(\varpi)$ bit chunks, where ϖ denotes the modulation order, and then, each chunk is emitted and modulated over FSO and RF links, respectively. Additionally, the RF systems are operated on the *mm*Wave bands to provide equal bandwidth to exploit the diversity. Furthermore, we employ two well-known AF relaying schemes during data transmission. In the AF relay methods, the power amplification operation is on the basis of partial and full channel state information of the source-relay and relay-destination channels, called as, fixed- and variable-gain AF relaying methods, respectively.

A. CHANNEL CHARACTERISTICS

The captured optical irradiance of FSO links can statistically be characterized with the aid of Gamma-Gamma atmospheric turbulence model. This distribution has been extensively considered to characterize the behavior of FSO communication channels in the open literature. This is because of its double random scintillation structure, where the captured laser intensity consists of multiplication of two Gamma random variables (RVs) to model the irradiation variation resulting from small-scale and large-scale atmospheric behavior [2], [43], [44]. Therefore, the RV I is used to present the instantaneous FSO turbulence gain which has Gamma-Gamma distribution. Taking the pointing error impairments into account, the related probability density function (PDF) is given as [43, (57)]

$$f_I(i) = \frac{\xi^2}{i\Gamma(\alpha)\Gamma(\beta)} G_{1,3}^{3,0}\left(\alpha\beta i \,\middle|\, \begin{matrix} \xi^2+1 \\ \xi^2, \alpha, \beta \end{matrix}\right), \tag{1}$$

where i is greater than zero by definition, $\Gamma(\cdot)$ depicts the Gamma function, $G_{\cdot,\cdot}^{\cdot,\cdot}(\cdot)$ represents the Meijer's G function, and ξ denotes the ratio between the equivalent beam radius and the pointing error displacement standard deviation, called as jitter. Notice that the impact of pointing errors is considered as negligible when $\xi \to \infty$. The variables α and β present the small-scale and large-scale coefficients, respectively, which can be obtained as [43, (58)-(59)]

$$\alpha = \exp\left\{\exp\left[\frac{0.49\zeta^2}{\left(1+0.65\vartheta^2+1.11\zeta^{12/5}\right)^{7/6}}\right]-1\right\}^{-1}, \tag{2}$$

$$\beta = \exp\left\{\exp\left[\frac{0.51\zeta^2\left(1+0.69\zeta^{12/5}\right)^{-5/6}}{1+0.9\vartheta^2+0.62\vartheta^2\zeta^{12/5}}\right]-1\right\}^{-1}, \tag{3}$$

where the Rytov variance is given by $\zeta^2 = 1.23C_n^2\Lambda^{7/6}d^{11/6}$, and $\vartheta = \sqrt{\Lambda A^2/4d}$. Additionally, $\Lambda = 2\pi/\lambda_o$ depicts the optical wave number, λ_o is the optical carrier wavelength, d stands for the communication link distance, A represents the aperture diameter of the lens, and C_n^2 denotes the atmospheric deflective indicator (also called as turbulence strength), which is generally obtained by the Hufnagel-Valley (HV5/7) profile [44]. It is worthy to note that another widely used atmospheric turbulence model for FSO systems is well-known Málaga distribution. Since the density functions of Gamma-Gamma and Málaga distributions are in the same form with different parameters, the analytical method adopted in this study can be directly applied for an FSO system that is modeled by the Málaga distribution [35], [45].

The statistical behavior of small-scale fading of *mm*Wave[1] bands has not been extensively investigated in the open literature, in comparison with the large-scale path loss model [48]–[50]. Higher (beyond 6 GHz) *mm*Wave channel models that are provided by the 3GPP organization for the 5G standard are considered as mathematically intractable [51].

[1] In the current literature, more complex channel models have been proposed for *mm*Wave systems [20], [46], [47]. However, Nakagami-*m* distribution is also widely adopted in modeling the *mm*Wave channel characteristics [48]–[54].

The experimental studies have lighten that small-scale fading behavior of *mm*Wave bands are highly depended on interference caused by temporal and spatial fading of multipath. Therefore, after a detailed literature search, Nakagami-*m* distribution is the most extensively used channel model to estimate the small-scale behavior of the *mm*Wave link [52]. Especially, 28 GHz and 60 GHz frequency bands can be accurately modeled by Nakagami-*m* distribution for several environmental and atmosphere condition, including clean and rainy weather conditions [52]–[54]. Therefore, the RV H is used to present the instantaneous RF fading gain which has Nakagami-*m* distribution. The related PDF is well-known and given as

$$f_H(h) = \frac{2m^m}{\Gamma(m)} h^{2m-1} e^{-mh^2}, \tag{4}$$

where m stands for the fading severity (order).

B. SIGNAL-TO-NOISE RATIOS

Relay and destination nodes uses the maximum ratio combining (MRC) diversity technique on the captured signals through RF and FSO systems, where the subscript $x \in \{1, 2\}$ represents receiver node, i.e., $x = 1$ for the first hop, and $x = 2$ for the second hop. Therefore, in each hop, the total electrical SNR is calculated by summing the instantaneous electrical SNRs for MRC receiver

$$\gamma_x = \gamma_{x,o} + \gamma_{x,f}, \tag{5}$$

where $\gamma_{x,o}$ and $\gamma_{x,f}$ are the instantaneous electrical SNR of FSO and RF links, respectively.

The expression of $\gamma_{x,o}$ is given as

$$\gamma_{x,o} = \Upsilon_{\tau,x} I_x^2, \tag{6}$$

where I_x depicts the normalized irradiation, $\Upsilon_{\tau,x}$ denotes the average electrical SNR received from the FSO link, and the parameter $\tau \in \{1, 2\}$ defines the optical signal detection technique, i.e., $\tau = 1$ indicates the heterodyne detection ($\Upsilon_{1,x} = \Upsilon_{\text{Heterodyne}}$) while $\tau = 2$ indicates the IM/DD detection ($\Upsilon_{2,x} = \Upsilon_{\text{IM/DD}}$), defined as

$$\Upsilon_{1,x} = \overline{\gamma}_{x,o}, \quad \text{for } \tau = 1, \tag{7}$$

$$\Upsilon_{2,x} = \frac{\overline{\gamma}_{x,o}\alpha_x\beta_x(\xi_x^2+2)}{(\alpha_x+1)(\beta_x+1)(\xi_x^2+1)^2}, \quad \text{for } \tau = 2, \tag{8}$$

where

$$\overline{\gamma}_{x,o} = \left(\frac{\eta I_t L_{x,o}}{\sigma_x}\right)^2, \tag{9}$$

η is the conversion ratio from optical to electrical, I_t represents the radiant emittance, and $L_{x,o}$ is the intensity attenuation loss

$$L_{x,o} = \frac{\pi A^2}{4(\psi d_x)^2} \exp\left[-\varphi_o d_x\right], \tag{10}$$

where ψ depicts the beam divergence of the laser, A denotes the aperture diameter of photodetector, d_x stands for the link distance, and φ_o is the attenuation extinction coefficient.

Afterwards, by using a change of variable on the RV I in (1), the PDF of γ_o is obtained as

$$f_{\gamma_o}(\gamma_{x,o}) = \frac{\mathcal{P}_0(x)}{\gamma_{x,o}} G_{1,3}^{3,0}\left(\alpha_x\beta_x\left(\frac{\gamma_{x,o}}{\Upsilon_{\tau,x}}\right)^{\frac{1}{\tau}} \middle| \begin{matrix} \xi_x^2+1 \\ \xi_x^2, \alpha_x, \beta_x \end{matrix}\right), \tag{11}$$

then, its cumulative density function (CDF) is expressed as

$$F_{\gamma_o}(\gamma_{x,o}) = \mathcal{P}_1(x) G_{\tau+1,3\tau+1}^{3\tau,1}\left(\frac{(\alpha_x\beta_x)^\tau}{\tau^{2\tau}\Upsilon_{\tau,x}}\gamma_{x,o} \middle| \begin{matrix} 1, \mathcal{P}_2(x) \\ \mathcal{P}_3(x), 0 \end{matrix}\right). \tag{12}$$

where the parameters $\mathcal{P}_0(x)$, $\mathcal{P}_1(x)$, $\mathcal{P}_2(x)$ and $\mathcal{P}_3(x)$ are given as

$$\begin{aligned}
\mathcal{P}_0(x) &= \left(\xi_x^2\right)/\left(\tau\Gamma(\alpha_x)\Gamma(\beta_x)\right), \\
\mathcal{P}_1(x) &= \left(\tau^{\alpha_x+\beta_x-2}\xi_x^2\right)/\left((2\pi)^{\tau-1}\Gamma(\alpha_x)\Gamma(\beta_x)\right), \\
\mathcal{P}_2(x) &= \Delta(\tau, \xi_x^2+1), \\
\mathcal{P}_3(x) &= \Delta(\tau, \xi_x^2), \Delta(\tau, \alpha_x), \Delta(\tau, \beta_x).
\end{aligned}$$

Likewise, the expression of $\gamma_{x,f}$ is given as

$$\gamma_{x,f} = \overline{\gamma}_{x,f} H_x^2, \tag{13}$$

where H_x stands for the instantaneous channel power, $\overline{\gamma}_{x,f}$ represents the average electrical SNR of the RF link

$$\overline{\gamma}_{x,f} = \frac{P_t L_{x,f}}{\sigma_x^2}, \tag{14}$$

where P_t depicts the transmitting power, and $L_{x,f}$ denotes the path loss which is given as [52]

$$L_{x,f} = \frac{G_T G_R \lambda_f^2}{(4\pi d_x)^2(\varphi_{O_2} d_x)(\varphi_f d_x)}, \tag{15}$$

where G_T and G_R represent transmitting and receiving antenna gains, respectively. λ_f is the wavelength of RF carrier, and φ_{O_2} and φ_f denotes the oxygen and rain attenuation variables, respectively. As a rule of thumb, the instantaneous SNR of Nakagami-*m* channel gain given in (4) has a Gamma distribution, expressed as in [55, (2.21)]

$$f_{\gamma_f}(\gamma_{x,f}) = \frac{m_x^{m_x}}{\Gamma(m_x)\overline{\gamma}_{x,f}^{m_x}} \gamma_{x,f}^{m_x-1} \exp\left[-\frac{m_x}{\overline{\gamma}_{x,f}}\gamma_{x,f}\right], \tag{16}$$

then, its CDF is expressed as

$$F_{\gamma_f}(\gamma_{x,f}) = \frac{1}{\Gamma(m_x)}\Gamma_{\text{L}}\left(m_x, \frac{\gamma_{x,f}}{\overline{\gamma}_{x,f}}\right), \tag{17}$$

where $\Gamma_{\text{L}}(\cdot,\cdot)$ denotes the lower incomplete Gamma function, and alternatively, the CDF of SNR is re-expressed as

$$F_{\gamma_f}(\gamma_{x,f}) = 1 - \sum_{k=0}^{\infty} \frac{1}{k!}\left(\frac{m_x}{\overline{\gamma}_{x,f}}\right)^k \gamma_{x,f}^k \exp\left[-\frac{m_x}{\overline{\gamma}_{x,f}}\gamma_{x,f}\right], \tag{18}$$

$$= \frac{1}{\Gamma(m_x)} G_{1,2}^{1,1}\left(\frac{\gamma_{x,f}}{\overline{\gamma}_{x,f}} \middle| \begin{matrix} 1 \\ m_x, 0 \end{matrix}\right). \tag{19}$$

The asymptotic behavior of the CDF of RF link can be obtained by approximating the lower incomplete Gamma function as [56]

$$F_{\gamma_f}(\gamma_{x,f}) \approx \frac{1}{\Gamma(m_x+1)}\left(m_x\gamma_{x,f}^2\right)^{m_x}. \tag{20}$$

1) MIXED SNR OF A HOP

Since the overall SNR for each hop is given in (5), we can obtain the CDF of the overall SNR in each hop by using a simple variable transformation as follows. If we let $\Delta = \gamma_{x,o} + \gamma_{x,f}$, the CDF of Δ is expressed as

$$\begin{aligned} F_\Delta(\delta) &= \int_{-\infty}^{\infty}\int_{-\infty}^{\delta-\gamma_{x,f}} f_{\gamma_o}(\gamma_{x,o}) f_{\gamma_f}(\gamma_{x,f}) \cdot d\gamma_{x,o} d\gamma_{x,f}, \\ &= \int_0^{\infty} F_{\gamma_o}(\delta-\gamma_{x,f}) f_{\gamma_f}(\gamma_{x,f}) \cdot d\gamma_{x,f}, \end{aligned} \tag{21}$$

the integral in (21) is re-expressed by using (12) and (16)

$$\begin{aligned} F_\Delta(\delta) = \mathcal{P}_1(x)\frac{m_x^{m_x}}{\Gamma(m_x)\overline{\gamma}_{x,f}^{m_x}} \int_0^{\infty} \gamma_{x,f}^{m_x-1} e^{-\frac{m_x}{\overline{\gamma}_{x,f}}\gamma_{x,f}} \\ \times G_{\tau+1,3\tau+1}^{3\tau,1}\left(\frac{(\alpha_x\beta_x)^\tau}{\tau^{2\tau}\Upsilon_{\tau,x}}(\delta-\gamma_{x,f}) \middle| \begin{matrix} 1, \mathcal{P}_2(x) \\ \mathcal{P}_3(x), 0 \end{matrix}\right) \\ \cdot d\gamma_{x,f}, \end{aligned} \tag{22}$$

then, by letting $u = \delta - \gamma_{x,f}$, the integral is re-expressed as

$$\begin{aligned} F_\Delta(\delta) = -\mathcal{P}_1(x)\frac{m^m}{\Gamma(m)\overline{\gamma}_{x,f}^m} e^{-\frac{m}{\overline{\gamma}_{x,f}}\delta} \int_0^{\infty} (\delta-u)^{m-1} e^{\frac{m}{\overline{\gamma}_{x,f}}u} \\ \times G_{\tau+1,3\tau+1}^{3\tau,1}\left(\frac{(\alpha_x\beta_x)^\tau}{\tau^{2\tau}\Upsilon_{\tau,x}}u \middle| \begin{matrix} 1, \mathcal{P}_2(x) \\ \mathcal{P}_3(x), 0 \end{matrix}\right) \cdot du, \end{aligned} \tag{23}$$

here, the polynomial expression is re-organized by the aid of binomial expansion

$$(\delta-u)^{m-1} = \sum_{\ell=0}^{m-1}\binom{m-1}{\ell}\delta^{m-\ell-1}(-u)^\ell, \tag{24}$$

since the summation is upper limited by the parameter m_x of Nakagami-m distribution because of the binomial expansion, only the integer values of m_x are used in the results. Then, the integral is re-expressed as

$$\begin{aligned} F_\Delta(\delta) = -\mathcal{P}_1(x)\frac{m_x^{m_x}}{\Gamma(m_x)\overline{\gamma}_{x,f}^{m_x}} e^{-\frac{m_x}{\overline{\gamma}_{x,f}}\delta} \sum_{\ell=0}^{m_x-1}\binom{m_x-1}{\ell} \\ \times (-1)^\ell \delta^{m_x-\ell-1} \int_0^{\infty} u^\ell e^{\frac{m_x}{\overline{\gamma}_{x,f}}u} \\ \times G_{\tau+1,3\tau+1}^{3\tau,1}\left(\frac{(\alpha_x\beta_x)^\tau}{\tau^{2\tau}\Upsilon_{\tau,x}}u \middle| \begin{matrix} 1, \mathcal{P}_2(x) \\ \mathcal{P}_3(x), 0 \end{matrix}\right) \cdot du, \end{aligned} \tag{25}$$

and the integral is solved by using [57, (7.813-1)]

$$\begin{aligned} &F_\Delta(\delta) \\ &= \mathcal{P}_1(x)\frac{m_x^{m_x}}{\Gamma(m_x)\overline{\gamma}_{x,f}^{m_x}} e^{-\frac{m_x}{\overline{\gamma}_{x,f}}\delta} \sum_{\ell=0}^{m_x-1}\binom{m_x-1}{\ell}\delta^{m_x-\ell-1} \\ &\times \left(\frac{\overline{\gamma}_{x,f}}{m_x}\right)^{\ell+1} G_{\tau+2,3\tau+1}^{3\tau,2}\left(-\frac{(\alpha_x\beta_x)^\tau\overline{\gamma}_{x,f}}{\tau^{2\tau}m_x\Upsilon_{\tau,x}} \middle| \begin{matrix} -\ell, 1, \mathcal{P}_2(x) \\ \mathcal{P}_3(x), 0 \end{matrix}\right). \end{aligned} \tag{26}$$

further, by using a change of variable, (26) can be re-expressed as

$$F_\Delta(\delta) = C_0(x)\sum_{\ell=0}^{m_x-1} C_1(x)\delta^{m_x-\ell-1}e^{-\frac{m_x}{\overline{\gamma}_{x,f}}\delta}, \tag{27}$$

where

$$\begin{aligned} C_0(x) &= \mathcal{P}_1(x)\frac{m_x^{m_x}}{\Gamma(m_x)\overline{\gamma}_{x,f}^{m_x}}, \\ C_1(x) &= \binom{m_x-1}{\ell}\left(\frac{\overline{\gamma}_{x,f}}{m_x}\right)^{\ell+1} \\ &\quad \times G_{\tau+2,3\tau+1}^{3\tau,2}\left(-\frac{(\alpha_x\beta_x)^\tau\overline{\gamma}_{x,f}}{\tau^{2\tau}m_x\Upsilon_{\tau,x}} \middle| \begin{matrix} -\ell, 1, \mathcal{P}_2(x) \\ \mathcal{P}_3(x), 0 \end{matrix}\right). \end{aligned}$$

Accordingly, the PDF of the overall SNR in each hop is calculated as

$$\begin{aligned} f_\Delta(\delta) &= \frac{d}{d\delta}F_\Delta(\delta), \\ &= \frac{d}{d\delta}\left(C_0(x)\sum_{\ell=0}^{m_x-1} C_1(x)\delta^{m_x-\ell-1}e^{-\frac{m_x}{\overline{\gamma}_{x,f}}\delta}\right), \\ &= C_0(x)\sum_{\ell=0}^{m_x-1} C_1(x)(m_x-\ell-1)\delta^{m_x-\ell-2}e^{-\frac{m_x}{\overline{\gamma}_{x,f}}\delta} \\ &\quad - \frac{m_x}{\overline{\gamma}_{x,f}}\delta^{m_x-\ell-1}e^{-\frac{m_x}{\overline{\gamma}_{x,f}}\delta}. \end{aligned} \tag{28}$$

III. PERFORMANCE ANALYSIS

In this section outage probability and effective throughput are derived for the fixed-gain (FG) and variable-gain (VG) dual-hop relaying schemes.

A. OUTAGE PROBABILITY

The outage probability P_{out} is widely used to statistically characterize outage performance of a system when the overall end-to-end SNR of the system is lower than a predefined threshold value $\mathcal{R}$. It is defined as

$$\begin{aligned} P_{\text{out}}(\mathcal{R}) &= \text{Prob}\left(C < \mathcal{R}\right), \\ &= \text{Prob}\left(\mathcal{B}\log_2(1+\gamma_s) < \mathcal{R}\right), \\ &= \text{Prob}\left(\gamma_s < 2^{\mathcal{R}/\mathcal{B}} - 1\right), \end{aligned} \tag{29}$$

where the bandwidth is considered as unity, $\mathcal{B} = 1$, and therefore, the outage probability can be expressed in terms of the CDF of overall end-to-end system SNR

$$P_{\text{out}}(\mathcal{R}) = F_{\gamma_s}\left(2^{\mathcal{R}} - 1\right). \tag{30}$$

1) FIXED-GAIN RELAYING

In the fixed-gain relaying scheme, the received SNR at destination is expressed as

$$\gamma_s^{\text{FG}} = \frac{\gamma_1\gamma_2}{\gamma_2 + A}, \tag{31}$$

where A denotes the gain of relaying scheme. Accordingly, the CDF of the SNR at destination is expressed as

$$F_{\gamma_s}^{\mathrm{FG}}(\gamma_s) = \mathrm{Prob.}\left(\frac{\gamma_1\gamma_2}{\gamma_2 + A} \le \gamma_s\right), = \int_0^{\infty} F_{\gamma_1}\left(\left(1 + \frac{A}{\gamma_2}\right)\gamma_s\right) f_{\gamma_2}(\gamma_2) \cdot d\gamma_2. \quad (32)$$

the integral (32) is re-expressed by using (27) and (28)

$$F_{\gamma_s}^{\mathrm{FG}}(\gamma_s) = \int_0^{\infty} C_0(1) \sum_{\ell_1=0}^{m_1-1} C_1(1) \times \left(\gamma_s + \frac{A\gamma_s}{\gamma_2}\right)^{m_1-\ell_1-1} e^{-\frac{Am_1\gamma_s}{\overline{\gamma}_{1,f}\gamma_2} - \frac{m_1}{\overline{\gamma}_{1,f}}\gamma_s} \times C_0(2) \sum_{\ell_2=0}^{m_2-1} C_1(2) \left[(m_2 - \ell_2 - 1)\gamma_2^{m_2-\ell_2-2} \times e^{-\frac{m_2}{\overline{\gamma}_{2,f}}\gamma_2} - \frac{m_2}{\overline{\gamma}_{2,f}}\gamma_2^{m_2-\ell_2-1} e^{-\frac{m_2}{\overline{\gamma}_{2,f}}\gamma_2}\right] \cdot d\gamma_2, \quad (33)$$

by using binomial theorem, the polynomial term can be re-expressed as

$$\left(\gamma_s + \frac{A\gamma_s}{\gamma_2}\right)^{m_1-\ell_1-1} = \sum_{k=0}^{m_1-\ell_1-1} \binom{m_1 - \ell_1 - 1}{k} \times \gamma_s^{m_1-\ell_1-1} A^k \gamma_2^{-k}, \quad (34)$$

further, the integral (33) is re-expressed as

$$\begin{aligned} F_{\gamma_s}^{\mathrm{FG}}(\gamma_s) &= e^{-\frac{m_1}{\overline{\gamma}_{1,f}}\gamma_s} C_0(1) \sum_{\ell_1=0}^{m_1-1} C_1(1) C_0(2) \times \sum_{\ell_2=0}^{m_2-1} C_1(2) \sum_{k=0}^{m_1-\ell_1-1} \binom{m_1 - \ell_1 - 1}{k} A^k \gamma_s^{m_1-\ell_1-1} \\ &\times \left[(m_2 - \ell_2 - 1)\int_0^{\infty} \gamma_2^{m_2-\ell_2-k-2} e^{-\frac{m_1 A\gamma_s}{\overline{\gamma}_{1,f}\gamma_2} - \frac{m_2}{\overline{\gamma}_{2,f}}\gamma_2} \cdot d\gamma_2 \right. \\ &\left. - \frac{m_2}{\overline{\gamma}_{2,f}} \int_0^{\infty} \gamma_2^{m_2-\ell_2-k-1} e^{-\frac{m_1 A\gamma_s}{\overline{\gamma}_{1,f}\gamma_2} - \frac{m_2}{\overline{\gamma}_{2,f}}\gamma_2} \cdot d\gamma_2\right], \end{aligned} \quad (35)$$

thereafter, by using [58, (2.5.37-2)], the resultant integrals can be solved as in (36), as shown at the bottom of the page.

2) VARIABLE-GAIN RELAYING

shIn the variable-gain relaying scheme, the relay part exploits the channel state information and the received SNR at destination is expressed as

$$\gamma_s^{\mathrm{VG}} = \frac{\gamma_1\gamma_2}{\gamma_1 + \gamma_2 + 1} \approx \min(\gamma_1, \gamma_2), \quad (37)$$

and, the CDF of the SNR at destination is given as

$$\begin{aligned} F_{\gamma_s}^{\mathrm{VG}}(\gamma_s) &= \mathrm{Prob.}\big(\min(\gamma_1, \gamma_2 \le \gamma_1)\big) \\ &= F_{\gamma_1}(\gamma_s) + F_{\gamma_2}(\gamma_s) - F_{\gamma_1}(\gamma_s)F_{\gamma_2}(\gamma_s), \end{aligned} \quad (38)$$

then, by substituting (26) into (38), the CDF of the SNR at destination for variable-gain relaying is expressed as in (39), as shown at the bottom of the page.

B. ASYMPTOTIC OUTAGE PROBABILITY

1) FIXED-GAIN RELAYING

The asymptotic behavior of the outage probability for fixed-gain relaying scheme, given in (36), can be obtained as follows. It is well known that the modified Bessel function of the second kind can be approximated as [59]

$$K_a\left(2\sqrt{bx}\right) \approx \frac{|a|}{2}\left(\frac{1}{\sqrt{bx}}\right)^{|a|}. \quad (40)$$

Therefore, the asymptotic outage probability is expressed in (41), as given in the top of next page.

2) VARIABLE-GAIN RELAYING

The asymptotic behavior of the outage probability for variable-gain relaying scheme, given in (39), can be obtained as follows. The asymptote of a function of the form $f(x) = x^a e^{-bx}$ is obtained by the term $f_\infty(x) = x^a$, as given in [60]. Therefore, the asymptotic outage probability is expressed in (42), as given in the top of next page.

$$F_{\gamma_s}^{\mathrm{FG}}(\gamma_s) = 2e^{-\frac{m_1}{\overline{\gamma}_{1,f}}\gamma_s} C_0(1) \sum_{\ell_1=0}^{m_1-1} C_1(1) C_0(2) \sum_{\ell_2=0}^{m_2-1} C_1(2) \sum_{k=0}^{m_1-\ell_1-1} \binom{m_1 - \ell_1 - 1}{k} A^k \gamma_s^{m_1-\ell_1-1} \left(\frac{Am_1\overline{\gamma}_{2,f}}{m_2\overline{\gamma}_{1,f}}\gamma_s\right)^{\frac{m_2-\ell_2-k-1}{2}} \times \left[(m_2 - \ell_2 - 1)\left(\frac{m_2\overline{\gamma}_{1,f}}{Am_1\overline{\gamma}_{2,f}\gamma_s}\right) K_{m_2-\ell_2-k-2}\left(2\sqrt{\frac{Am_1m_2}{\overline{\gamma}_{1,f}\overline{\gamma}_{2,f}}\gamma_s}\right) - \frac{m_2}{\overline{\gamma}_{2,f}} K_{m_2-\ell_2-k-1}\left(2\sqrt{\frac{Am_1m_2}{\overline{\gamma}_{1,f}\overline{\gamma}_{2,f}}\gamma_s}\right)\right]. \quad (36)$$

$$F_{\gamma_s}^{\mathrm{VG}}(\gamma_s) = \mathcal{P}_1(1)\frac{m_1^{m_1}}{\Gamma(m_1)\overline{\gamma}_{1,f}^{m_1}} \sum_{\ell=0}^{m_1-1} C_1(1)\gamma_s^{m_1-\ell-1} e^{-\frac{m_1}{\overline{\gamma}_{1,f}}\gamma_s} + \mathcal{P}_1(2)\frac{m_2^{m_2}}{\Gamma(m_2)\overline{\gamma}_{2,f}^{m_2}} \sum_{\ell=0}^{m_2-1} C_1(2)\gamma_s^{m_2-\ell-1} e^{-\frac{m_2}{\overline{\gamma}_{2,f}}\gamma_s} \times \mathcal{P}_1(1)\frac{m_1^{m_1}}{\Gamma(m_1)\overline{\gamma}_{1,f}^{m_1}} \sum_{\ell=0}^{m_1-1} C_1(1)\gamma_s^{m_1-\ell-1} e^{-\frac{m_1}{\overline{\gamma}_{1,f}}\gamma_s} - \mathcal{P}_1(2)\frac{m_2^{m_2}}{\Gamma(m_2)\overline{\gamma}_{2,f}^{m_2}} \sum_{\ell=0}^{m_2-1} C_1(2)\gamma_s^{m_2-\ell-1} e^{-\frac{m_2}{\overline{\gamma}_{2,f}}\gamma_s} \quad (39)$$

C. EFFECTIVE THROUGHPUT

While conveying the information from source to destination over a relay, the system needs to satisfy a specific reliability level. To characterize this behavior of the system, we consider a metric called effective throughput T_{Eff}, which defined in terms of the outage probability, and it can be expressed as

$$T_{\text{Eff}}(\mathcal{R}) = \mathcal{R} \times \big(1 - P_{\text{out}}(\mathcal{R})\big). \tag{43}$$

1) FIXED-GAIN RELAYING

For the fixed-gain relaying scheme, the effective throughput is calculated by using overall end-to-end SNR

$$T_{\text{Eff}}^{\text{FG}}(\mathcal{R}) = \mathcal{R} \times \big(1 - F_{\gamma_s}^{\text{FG}}(2^{\mathcal{R}} - 1)\big). \tag{44}$$

where $F_{\gamma_s}^{\text{FG}}(\gamma_s)$ is given in (36).

2) VARIABLE-GAIN RELAYING

For the variable-gain relaying scheme, the effective throughput is calculated by using overall end-to-end SNR

$$T_{\text{Eff}}^{\text{VG}}(\mathcal{R}) = \mathcal{R} \times \big(1 - F_{\gamma_s}^{\text{VG}}(2^{\mathcal{R}} - 1)\big). \tag{45}$$

where $F_{\gamma_s}^{\text{VG}}(\gamma_s)$ is given in (39).

IV. RESULTS AND DISCUSSIONS

To present the analytical correctness of the proposed mathematical expressions in Section III, Monte-Carlo based simulations are given including related theoretical findings. Specifically, detailed investigations of the outage performance of dual-hop relaying hybrid FSO-*mm*Wave transmissions are presented in terms of the outage probability and effective throughput with the aid of PDFs and CDFs of overall end-to-end instantaneous SNRs. The results provided in this section include several cases which consists of different fundamental system variables like atmospheric conditions, relaying methods, link distances, and average SNRs. The Monte-Carlo simulation variables of the hybrid system and channel characteristics are presented in Table 1 and Table 2

TABLE 1. Physical layer parameters of FSO and *mm*Wave systems.

FSO System		
Variable	*Symbol*	*Value*
FSO Wavelength	λ_o	1550 nm
FSO Power	I_t	40 mW
Diameter of Aperture	A	0.2 m
Divergence of Beam	ψ	10 mrad
Photo-sensitivity	η	0.5 A/W
***m*mWave System**		
Variable	*Symbol*	*Value*
RF Wavelength	λ_f	$c/60$ nm
RF Power	P_t	10 mW
Gain of Transmitting Antenna	G_T	44 dBi
Gain of Receiving Antenna	G_R	44 dBi
Oxygen Absorption	φ_{O_2}	15.1 dB/km

* c denotes the speed of light.

TABLE 2. Parameters for different weather conditions.

Weather-Dependent Parameters			
Weather Conditions	υ_o *(dB/km)*	φ_{rain} *(dB/km)*	C_n^2
Clean Air	0.43	0	5×10^{-14}
Haze	4.2	0	1.7×10^{-14}
Moderate Rain (12.5 mm/h)	5.8	5.6	5×10^{-15}

[51], [52], [61]. For all finding, it is worthy to note that the average electrical SNR of each system is considered to be equal, where the electrical transmit power of the *mm*Wave system are fixed, and the optical transmit power of the FSO system are calculated.

A comparison of the outage performance of a relay-based dual-hop hybrid FSO-RF system as a function of the average SNR at first- and second-hop is illustrated in Figs. 2 and 3 for heterodyne and IM/DD detection techniques, respectively. The performance results of single-hop hybrid and dual-hop mixed FSO-RF system are also included as a benchmark. The performance of two well-known AF relaying scheme are

$$\begin{aligned} F_{\gamma_s,\infty}^{\text{FG}}(\gamma_s) = {} & e^{-\frac{m_1}{\overline{\gamma}_{1,f}}\gamma_s} C_0(1) \sum_{\ell_1=0}^{m_1-1} C_1(1) C_0(2) \sum_{\ell_2=0}^{m_2-1} C_1(2) \sum_{k=0}^{m_1-\ell_1-1} \binom{m_1-\ell_1-1}{k} A^k \frac{m_2}{\overline{\gamma}_{2,f}} \left(\frac{A m_1 \overline{\gamma}_{2,f}}{m_2 \overline{\gamma}_{1,f}}\right)^{\frac{m_2-\ell_2-k-1}{2}} \\ & \times \left[\frac{|m_2-\ell_2-k-2|(m_2-\ell_2-1)\overline{\gamma}_{1,f}}{m_1 A} \gamma_s^{\frac{2m_1+m_2-2\ell_1-\ell_2-k-5}{2}} \left(\sqrt{\frac{\overline{\gamma}_{1,f}\overline{\gamma}_{2,f}}{A m_1 m_2 \gamma_s}}\right)^{|m_2-\ell_2-k-2|} \right. \\ & \left. - (m_2-\ell_2-k-1) \left(\sqrt{\frac{\overline{\gamma}_{1,f}\overline{\gamma}_{2,f}}{A m_1 m_2}}\right)^{m_2-\ell_2-k-1} \gamma_s^{\frac{2m_1-m_2-2\ell_1+\ell_2+k-1}{2}} \right]. \end{aligned} \tag{41}$$

$$\begin{aligned} F_{\gamma_s,\infty}^{\text{VG}}(\gamma_s) = {} & \mathcal{P}_1(1) \frac{m_1^{m_1}}{\Gamma(m_1)\overline{\gamma}_{1,f}^{m_1}} \sum_{\ell=0}^{m_1-1} C_1(1) \gamma_s^{m_1-\ell-1} + \mathcal{P}_1(2) \frac{m_2^{m_2}}{\Gamma(m_2)\overline{\gamma}_{2,f}^{m_2}} \sum_{\ell=0}^{m_2-1} C_1(2) \gamma_s^{m_2-\ell-1} \\ & \times \mathcal{P}_1(1) \frac{m_1^{m_1}}{\Gamma(m_1)\overline{\gamma}_{1,f}^{m_1}} \sum_{\ell=0}^{m_1-1} C_1(1) \gamma_s^{m_1-\ell-1} - \mathcal{P}_1(2) \frac{m_2^{m_2}}{\Gamma(m_2)\overline{\gamma}_{2,f}^{m_2}} \sum_{\ell=0}^{m_2-1} C_1(2) \gamma_s^{m_2-\ell-1} \end{aligned} \tag{42}$$

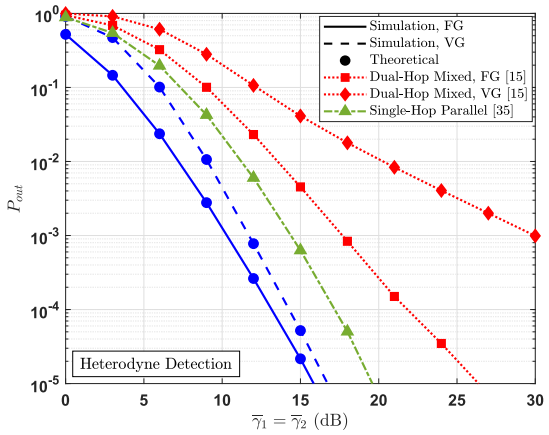

FIGURE 2. A comparison of outage probability as a function of overall system SNR for proposed and reference studies. (Clean weather, $\xi = 1.1$, $\mathcal{R} = 1$ bit, $d_1 = d_2 = 1.25$ km, $m_1 = m_2 = 1$, $\alpha_1 = \alpha_2 = 3.58$, $\beta_1 = \beta_2 = 3.33$, $A = 0.5$.)

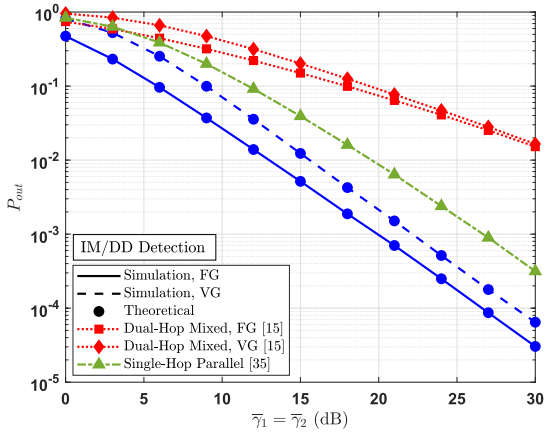

FIGURE 3. A comparison of outage probability as a function of overall system SNR for proposed and reference studies. (Clean weather, $\xi = 1.1$, $\mathcal{R} = 1$ bit, $d_1 = d_2 = 1.25$ km, $m_1 = m_2 = 1$, $\alpha_1 = \alpha_2 = 3.58$, $\beta_1 = \beta_2 = 3.33$, $A = 0.5$.)

illustrated in clean weather conditions, where the distance in first hop d_1 and second hop d_2 is assumed to be the same as 1.25 km. Additionally, the gain A is set to 0.5 for fixed-gain relaying scheme. Since we consider the same distance and weather condition in each hop, the turbulence parameters are calculated as $\alpha_1 = \alpha_2 = 3.58$, $\beta_1 = \beta_2 = 3.33$, where the Nakagami-m parameter is set to $m_1 = m_2 = 1$. Also, the threshold of outage probability is considered as $\mathcal{R} = 1$ bit. As expected, the fixed-gain scheme performs better than the variable-gain, since fixed-gain scheme exploits the full channel state information. Additionally, it can easily seen from the figure that the proposed dual-hop system outperforms the single-hop parallel and dual-hop mixed hybrid systems for both fixed-gain and variable-gain relay methods including heterodyne and IM/DD detection techniques. For instance, considering the heterodyne detection in FSO link, at a fixed end-to-end SNR of 15 dB, the proposed system experience outage with probabilities of 2×10^{-5} and 5×10^{-5} for fixed-gain and variable-gain, respectively, where these probabilities are 3×10^{-3} and 3×10^{-3} for dual-hop mixed system. Additionally, single-hop parallel system provides an outage probability of 5×10^{-4}. It is clear from the figures that the proposed relay-based dual-hop hybrid system outperforms both benchmark systems for heterodyne and IM/DD detection techniques.

In Figs. 4 and 5, the outage probability of the proposed dual-hop hybrid system is investigated for the fixed average SNR of each link, i.e., the average SNR of the first-hop is fixed at 12 dB in Fig. 4, and the average SNR of the second-hop is fixed at 12 dB in Fig. 5. In the figures, the impact of different weather conditions on the outage performance is examined for both fixed- and variable-gain relaying schemes over a distance of 1.5 km in each hop, considering a pointing error of $\xi = 6.7$ in FSO links, and the outage threshold is set to $\mathcal{R} = 2$ bits. It obvious that the weather conditions have significant effects on the system's outage performance for both detection techniques. When the weather

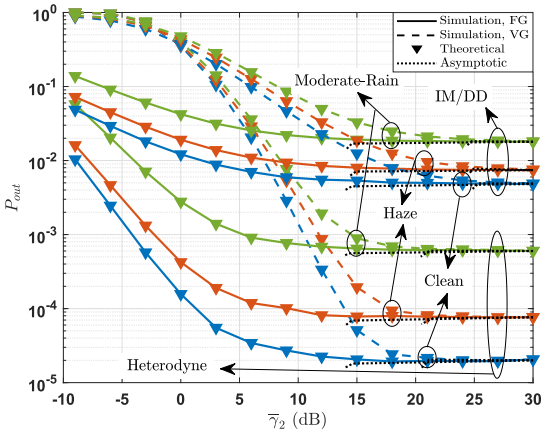

FIGURE 4. The probability of outage as a function of overall system SNR for different weather conditions. ($\xi = 6.7$, $d_1 = d_2 = 1.5$ km, $m_1 = m_2 = 1$, $A = 0.5$, $\mathcal{R} = 2$ bits, $\overline{\gamma}_1 = 12$ dB).

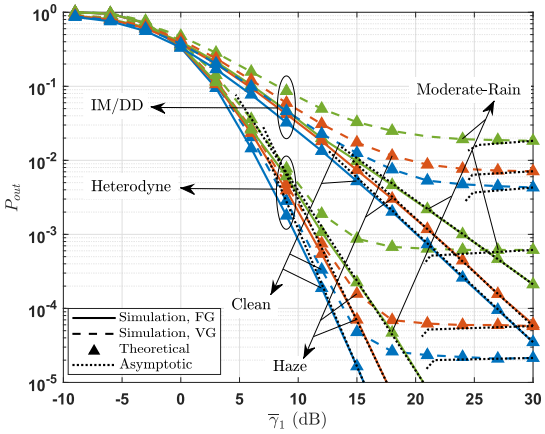

FIGURE 5. The probability of outage as a function of overall system SNR for different weather conditions. ($\xi = 6.7$, $d_1 = d_2 = 1.5$ km, $m_1 = m_2 = 1$, $A = 0.5$, $\mathcal{R} = 2$ bits, $\overline{\gamma}_2 = 12$ dB).

conditions become more severe, i.e., from clean to moderate rain, the transmission reliability decreases significantly. For example, in Fig. 4, considering a fixed average SNR of $\overline{\gamma}_2 = 20\,\text{dB}$, the expected outage probabilities are 2×10^{-5}, 8×10^{-5} and 5×10^{-4} for clean, hazy and moderate rain weather conditions, respectively, with heterodyne detection. These number are, in turn, approximately 5×10^{-3}, 8×10^{-3} and 2×10^{-2} for IM/DD detection technique. Furthermore, in comparison between Figs. 4 and 5, one can easily observe the importance of the average SNR in the first-hop for fixed-gain AF relaying scheme. Since the amplification process directly depends on the received SNR at the relay node, the SNR of first-hop plays an important role on the outage performance for fixed-gain scheme. For instance, limiting the SNR in the first-hop creates a kind of noise floor, which results in a saturation in the reliability, and therefore, the outage performance cannot be improved beyond 10^{-5} for heterodyne detection in a clean weather condition, as seen in Fig. 4. However, increasing the SNR in the first-hop and limiting the SNR in the second-hop does not result in the same outage behavior for fixed-gain but for variable-gain AF relaying scheme. This is because of the variable-scheme technique always utilizes the lowest SNR of both hops.

The outage probability of the proposed dual-hop hybrid system is illustrated for the fixed distance in each link considering different pointing errors, i.e., the distance in the first-hop is fixed at 1 km in Fig. 6, and the distance in the second-hop is fixed at 1 km in Fig. 7. The effect of pointing errors in FSO links on the outage performance is investigated for both fixed- and variable-gain schemes at fixed average SNR of $\overline{\gamma}_1 = \overline{\gamma}_2 = 10\,\text{dB}$ in hazy weather conditions, and the outage threshold is set to $\mathcal{R} = 2$ bits. From the figures, it can be observed that the pointing errors have remarkable influence on the outage probability for heterodyne technique. Recalling that $\xi \to \infty$ implies no pointing errors in the system, a decrease in the value of ξ, which means an increase in the pointing error, dramatically reduce the overall reliability

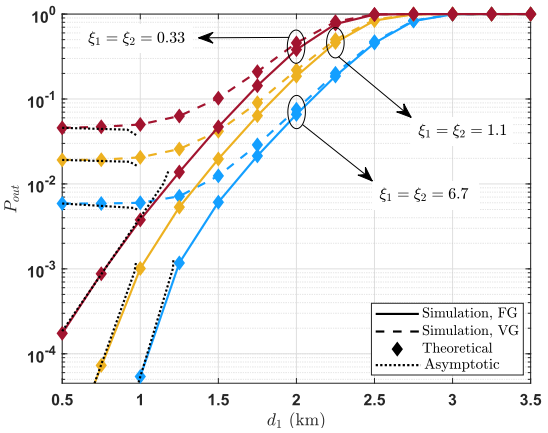

FIGURE 7. The impact of pointing error on the outage performance as a function of distance in first-hop. (Hazy weather, $m_1 = m_2 = 1$, $A = 0.5$, $\mathcal{R} = 2$ bits, $\overline{\gamma}_1 = \overline{\gamma}_2 = 15\,\text{dB}$, $d_2 = 1.5\,\text{km}$.)

of the transmission. It is worth to note that the values of the pointing errors are adopted from reference studies [21], [33]. For instance, in Fig. 6, considering a distance of $d_2 = 1\,\text{km}$, the probabilities of transmission outage with fixed-gain relay scheme are 2×10^{-4}, 1×10^{-3} and 4×10^{-3} for the pointing errors of 6.7, 1.1 and 0.33, respectively. On the other hand, in Fig. 7, considering a distance of $d_1 = 1\,\text{km}$, these probabilities can be obtained as 5×10^{-5}, 1×10^{-3} and 4×10^{-3} for the pointing errors of 6.7, 1.1 and 0.33, respectively. Notice that the both scenarios provides approximately identical outage probabilities, however, when we look at the fixed distance lower than 1 km, we observe that the outage performance is not saturated and can be lower in comparison with higher distances. As in the previous two figures, this behavior, also, directly related with average SNR in the first-hop, since lowering the distance results in a higher SNR value.

The outage performance as a function of the overall end-to-end SNR at destination is represented in Fig. 8, considering the impact of several atmospheric circumstances on the

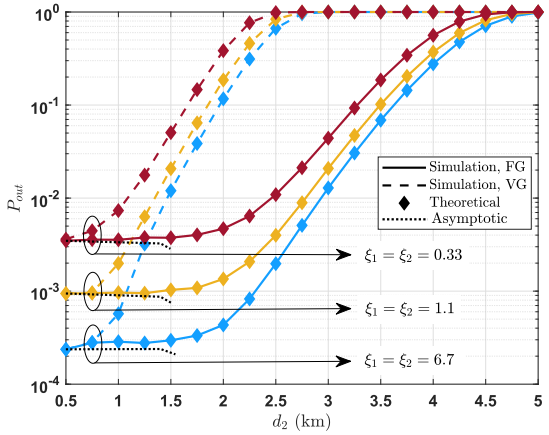

FIGURE 6. The impact of pointing error on the outage performance as a function of distance in second-hop. (Hazy weather, $m_1 = m_2 = 1$, $A = 0.5$, $\mathcal{R} = 2$ bits, $\overline{\gamma}_1 = \overline{\gamma}_2 = 10\,\text{dB}$, $d_1 = 1\,\text{km}$.)

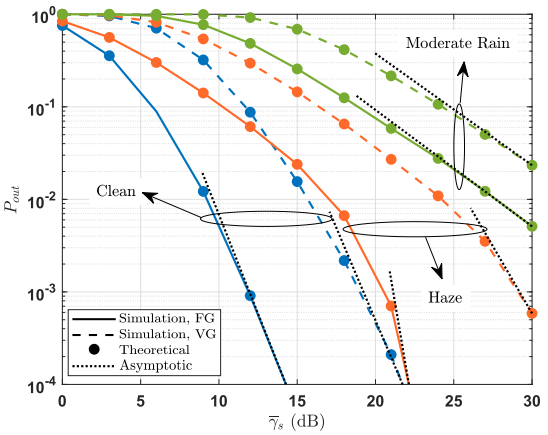

FIGURE 8. The probability of outage as a function of overall system SNR for different weather conditions. ($\xi = 6.7$, $d_1 = 1\,\text{km}$, $d_2 = 1.25\,\text{km}$, $m_1 = m_2 = 1$, $A = 0.5$, $\mathcal{R} = 2$ bits).

system, with distance of $d_1 = 1$ km in the first hop and of $d_2 = 1.25$ km in the second hop. Nakagami-m parameters are set to $m_1 = m_2 = 1$. The turbulence parameters in the first hop are calculated as $\{\alpha_1 = 5.0096, \beta_1 = 4.7489\}$, $\{\alpha_1 = 14.6608, \beta_1 = 14.0573\}$ and $\{\alpha_1 = 50.7685, \beta_1 = 48.7564\}$ for clean, hazy and moderate rain weather conditions, where they are, in turn, calculated as $\{\alpha_2 = 3.5848, \beta_2 = 3.3349\}$, $\{\alpha_2 = 9.6652, \beta_2 = 9.2504\}$ and $\{\alpha_2 = 33.5727, \beta_2 = 32.2337\}$ for the second hop. As it is seen from the figure, the reliability performance is heavily degraded for weather conditions when it goes from clean to moderate rain for both schemes. For each weather scenario, the variable-gain relaying scheme mostly performs lower outage probability compared to fixed-gain scheme. To express it in a different way, regardless of a weather condition, variable-gain relaying provides better quality of service since it exploits the full channel state information. For instance, if we want to achieve a reliable communication with a probability of 10^{-2}, the minimum overall end-to-end SNR pair for variable- and fixed-gain schemes needs to approximately be $\{9, 16\}$, $\{9, 16\}$ and $\{9, 16\}$ dB for clean, hazy and moderate rain weather conditions, respectively.

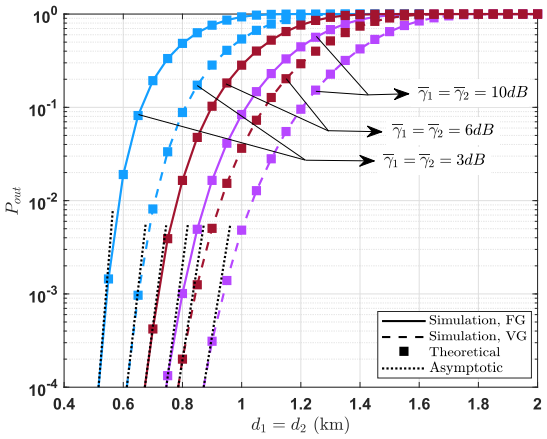

FIGURE 9. The probability of outage as a function of distances in the first- and second-hops for different fixed average SNRs with heterodyne. (Hazy weather, $\xi = 6.7$, $m_1 = m_2 = 1$, $A = 0.5$, $\mathcal{R} = 1$ bit.)

Alternatively, in Fig. 9, the probability of outage as a function of the distance is illustrated for different fixed overall end-to-end SNR in hazy weather conditions. The distance in first hop d_1 and in second hop d_2 is assumed to be the same as variable, and the threshold of outage probability is considered as $\mathcal{R} = 1$ bit. Since the distances d_1 and d_2 change for each case, the turbulence parameters α_1, β_1, α_2 and β_2 needs to be calculated separately based on (2) and (3), where Nakagami-m parameters are set to $m_1 = m_2 = 1$. The impact of end-to-end SNR can be easily observed from the figure, in which the higher overall SNR results in more reliable communication system for each fixed- and variable-gain relaying schemes. For example, if we are required to satisfy at most 10^{-2} outage performance, the distance pair for fixed- and variable-gain schemes in each hop approximately needs to be $\{600, 700\}$ m, $\{800, 950\}$ m, and $\{900, 1050\}$ m for the fixed end-to-end SNRs of 3, 6 and 10 dB, respectively.

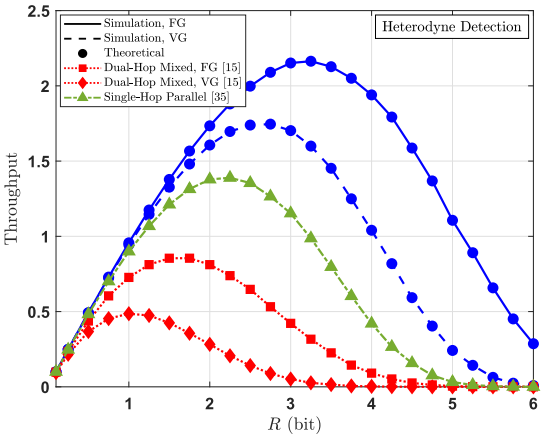

FIGURE 10. A comparison of effective throughput as a function of outage probability threshold with heterodyne detection for the proposed and the reference studies. (Haze weather, $\xi = 1.1$, $d_1 = 1$ km, $d_2 = 1.25$ km, $\gamma_1 = 10$ dB, $\gamma_2 = 15$ dB, $\alpha_1 = 14.6608$, $\beta_1 = 14.0573$, $\alpha_2 = 10.4284$, $\beta_2 = 9.9853$, $m_1 = m_2 = 1$, $A = 0.5$.)

A comparison of the effective throughput metric as a function of the outage probability threshold is illustrated in Figs. 10 and 11 for two different relaying schemes to illustrate the outage performance of the proposed and the benchmark systems in hazy weather conditions. The distance in first hop d_1 and second hop d_2 is assumed to be 1 km and 1.25 km, respectively, while the Nakagami-m parameters are set to $m_1 = m_2 = 1$. Additionally, the turbulence parameters are calculated as $\alpha_1 = 14.6608$, $\beta_1 = 14.0573$, $\alpha_2 = 10.4284$, and $\beta_2 = 9.9853$. From the figure, we can easily observe that the proposed relaying system outperforms the benchmark system for both fixed-gain and variable-gain relaying schemes. For instance, if we consider an outage threshold of $\mathcal{R} = 2$ bits, for fixed- and variable-gain schemes,

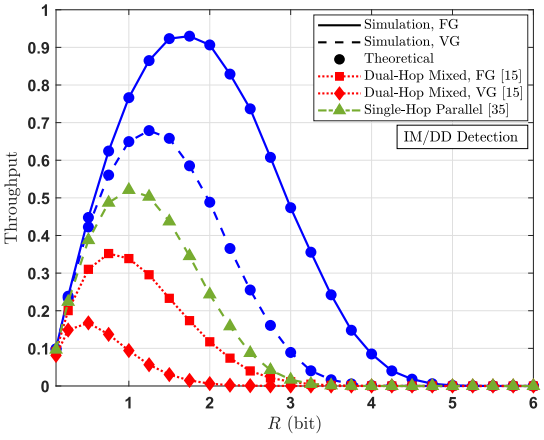

FIGURE 11. A comparison of effective throughput as a function of outage probability threshold with IM/DD detection for the proposed and the reference studies. (Haze weather, $\xi = 1.1$, $d_1 = 1$ km, $d_2 = 1.25$ km, $\gamma_1 = 10$ dB, $\gamma_2 = 15$ dB, $\alpha_1 = 14.6608$, $\beta_1 = 14.0573$, $\alpha_2 = 10.4284$, $\beta_2 = 9.9853$, $m_1 = m_2 = 1$, $A = 0.5$.)

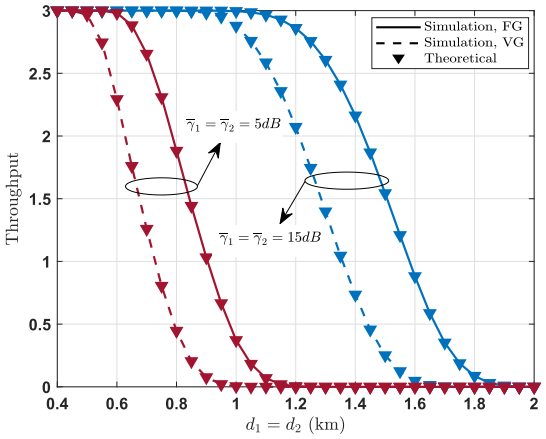

FIGURE 12. The effective throughput as a function of distances in the first- and second-hops for different fixed average SNRs with heterodyne. (Clean weather, $\xi = 1.1$, $m_1 = m_2 = 2$, $A = 0.5$, $\mathcal{R} = 3$ bits.)

the proposed and benchmark systems are able to satisfy the pair of effective throughput $\{1.6072, 1.7345\}$ bits and $\{0.2823, 0.8118\}$ bits, respectively, and additionally, if we consider an outage threshold of $\mathcal{R} = 3$ bits, these numbers are $\{1.7037, 2.1528\}$ bits and $\{0.0519, 0.4218\}$ bits, respectively. Moreover, we can observe that the effective throughput illustrates a non-monotonic behavior with the increase of outage threshold $\mathcal{R}$. In other words, when we increase the outage threshold, the effective throughput starts increasing, and then, it begins decreasing. We can explain this behavior as follows: the increment in outage threshold is higher than the increase in probability of outage, and therefore, effective throughput increases with the increase in threshold. However, after a specific value of threshold, the outage probability becomes dominant, and it dramatically increase the effective throughput.

Effective throughput as a function of link distances is represented in Fig. 12 for different fixed overall end-to-end SNR in clean weather conditions. The distance in first hop d_1 and in second hop d_2 is assumed to be the same as variable, and the threshold of outage probability is considered as $\mathcal{R} = 3$ bits, where Nakagami-m parameters are set to $m_1 = m_2 = 2$. The impact of end-to-end SNR on the effective throughput can be easily observed from the figure. For instance, if we need to satisfy an effective throughput of 2 bits, the distance pair for fixed- and variable-gain schemes in each hop approximately needs to be $\{650, 800\}$ m and $\{1200, 1450\}$ m for the fixed end-to-end SNRs of 5 and 15 dB, respectively.

V. CONCLUSION

In this study, the outage performance of relay-based dual-hop hybrid FSO-*mm*Wave systems is investigated for fixed- and variable-gain relaying transmissions. Specifically, the transmissions in each hop is established through optical gamma-gamma atmospheric turbulence and *mm*Wave Nakagami-m fading channels at the same time, and the MRC diversity combining method is used at the relay and destination receivers. As performance metrics, the outage probability and effective throughput are derived for fixed- and variable-gain relaying schemes. Additionally, the impact of different fundamental physical layer parameters on the transmission reliability are examined for two relay methods. As explained previously, the nature of relay-based dual-hop mixed FSO-RF systems demonstrate that the overall system performance can be significantly degraded by either FSO and/or RF links due to the adverse weather conditions. However, the utilization of hybrid FSO-RF links in each data transmission hop can overcome this problem due to the complementary properties of RF and FSO systems. Analytical findings which are discussed allow us to explain how reliable transmission and reception can be made in several cases of interest in the context of hybrid FSO-*mm*Wave systems. In view of the findings, relay-based dual-hop hybrid FSO-*mm*Wave transmissions can be considered for the design of more reliable communication systems due to their distinctive behavior under different atmospheric conditions. Furthermore, by illustrating the effects of various atmospheric turbulence conditions on each hop and link, the utilization of a hybrid transmission remarkably decrease the outage performance of dual-hop relays. Moreover, both FSO and *mm*Wave systems are able to satisfy the low latency, ultra reliability, and high capacity requirements of 5G and beyond networks. As a conclusion, the examination provided in this work can be useful in the process of system design to build more reliable data transmission under several scenarios.

REFERENCES

[1] Y. Wang, J. Li, L. Huang, Y. Jing, A. Georgakopoulos, and P. Demestichas, "5G mobile: Spectrum broadening to higher-frequency bands to support high data rates," *IEEE Veh. Technol. Mag.*, vol. 9, no. 3, pp. 39–46, Sep. 2014.

[2] M. A. Khalighi and M. Uysal, "Survey on free space optical communication: A communication theory perspective," *IEEE Commun. Surveys Tuts.*, vol. 16, no. 4, pp. 2231–2258, Jun. 2014.

[3] A. Vavoulas, H. G. Sandalidis, and D. Varoutas, "Weather effects on FSO network connectivity," *J. Opt. Commun. Netw.*, vol. 4, no. 10, pp. 734–740, Oct. 2012.

[4] S. Althunibat, Z. Altarawneh, and R. Mesleh, "Performance analysis of free space optical–based wireless sensor networks using corner cube retroreflectors," *Trans. Emerg. Telecommun. Technol.*, vol. 30, no. 12, p. e3707, Dec. 2019.

[5] Z. Pi and F. Khan, "An introduction to millimeter-wave mobile broadband systems," *IEEE Commun. Mag.*, vol. 49, no. 6, pp. 101–107, Jun. 2011.

[6] J. Antes, F. Boes, T. Messinger, U. J. Lewark, T. Mahler, A. Tessmann, R. Henneberger, T. Zwick, and I. Kallfass, "Multi-gigabit millimeter-wave wireless communication in realistic transmission environments," *IEEE Trans. THz Sci. Technol.*, vol. 5, no. 6, pp. 1078–1087, Nov. 2015.

[7] R. Boluda-Ruiz, S. C. Tokgoz, A. Garcia-Zambrana, and K. Qaraqe, "Asymptotic average secrecy rate for MISO free-space optical wiretap channels," in *Proc. IEEE 20th Int. Workshop Signal Process. Adv. Wireless Commun. (SPAWC)*, Jul. 2019, pp. 1–5.

[8] S. C. Tokgoz, S. Althunibat, S. L. Miller, and K. A. Qaraqe, "Performance analysis of index modulation based link-selection mechanism for hybrid FSO-mmWave systems," *Opt. Commun.*, vol. 479, Jan. 2021, Art. no. 126305.

[9] M. A. Hasabelnaby, H. A. I. Selmy, and M. I. Dessouky, "Joint optimal transceiver placement and resource allocation schemes for redirected cooperative hybrid FSO/mmW 5G fronthaul networks," *J. Opt. Commun. Netw.*, vol. 10, no. 12, pp. 975–990, Dec. 2018.

[10] S. C. Tokgoz, S. Althunibat, and K. Qaraqe, "A link-selection mechanism for hybrid FSO-mmWave systems based on index modulation," in *Proc. IEEE Int. Conf. Commun. (ICC)*, Jun. 2020, pp. 1–7.
[11] S. Althunibat, O. S. Badarneh, R. Mesleh, and K. Qaraqe, "A hybrid free space optical-millimeter wave cooperative system," *Opt. Commun.*, vol. 453, Dec. 2019, Art. no. 124400.
[12] Q. Sun, Z. Zhang, Y. Zhang, M. López-Benítez, and J. Zhang, "Performance analysis of dual-hop wireless systems over mixed FSO/RF fading channel," *IEEE Access*, vol. 9, pp. 85529–85542, 2021.
[13] E. Lee, J. Park, D. Han, and G. Yoon, "Performance analysis of the asymmetric dual-hop relay transmission with mixed RF/FSO links," *IEEE Photon. Technol. Lett.*, vol. 23, no. 21, pp. 1642–1644, Nov. 1, 2011.
[14] I. S. Ansari, F. Yilmaz, and M.-S. Alouini, "Impact of pointing errors on the performance of mixed RF/FSO dual-hop transmission systems," *IEEE Wireless Commun. Lett.*, vol. 2, no. 3, pp. 351–354, Jun. 2013.
[15] E. Zedini, I. S. Ansari, and M.-S. Alouini, "Performance analysis of mixed Nakagami-*m* and gamma-gamma dual-hop FSO transmission systems," *IEEE Photon. J.*, vol. 7, no. 1, pp. 1–20, Dec. 2015.
[16] E. Zedini, H. Soury, and M.-S. Alouini, "On the performance analysis of dual-hop mixed FSO/RF systems," *IEEE Trans. Wireless Commun.*, vol. 15, no. 5, pp. 3679–3689, May 2016.
[17] S. Anees and M. R. Bhatnagar, "Performance of an amplify-and-forward dual-hop asymmetric RF-FSO communication system," *J. Opt. Commun. Netw.*, vol. 7, no. 2, pp. 124–135, 2015.
[18] L. Yang, M. O. Hasna, and X. Gao, "Performance of mixed RF/FSO with variable gain over generalized atmospheric turbulence channels," *IEEE J. Sel. Areas Commun.*, vol. 33, no. 9, pp. 1913–1924, Sep. 2015.
[19] L. Kong, W. Xu, L. Hanzo, H. Zhang, and C. Zhao, "Performance of a free-space-optical relay-assisted hybrid RF/FSO system in generalized M-distributed channels," *IEEE Photon. J.*, vol. 7, no. 5, pp. 1–19, Oct. 2015.
[20] I. S. Ansari, M.-S. Alouini, and F. Yilmaz, "On the performance of hybrid RF and RF/FSO fixed gain dual-hop transmission systems," in *Proc. Saudi Int. Electron., Commun. Photon. Conf.*, Apr. 2013, pp. 1–6.
[21] G. N. Kamga, S. Aissa, T. R. Rasethuntsa, and M.-S. Alouini, "Mixed RF/FSO communications with outdated-CSI-based relay selection under double generalized gamma turbulence, generalized pointing errors, and Nakagami-m fading," *IEEE Trans. Wireless Commun.*, vol. 20, no. 5, pp. 2761–2775, May 2021.
[22] E. Balti, M. Guizani, B. Hamdaoui, and B. Khalfi, "Aggregate hardware impairments over mixed RF/FSO relaying systems with outdated CSI," *IEEE Trans. Commun.*, vol. 66, no. 3, pp. 1110–1123, Mar. 2018.
[23] G. T. Djordjevic, M. I. Petkovic, A. M. Cvetkovic, and G. K. Karagiannidis, "Mixed RF/FSO relaying with outdated channel state information," *IEEE J. Sel. Areas Commun.*, vol. 33, no. 9, pp. 1935–1948, Sep. 2015.
[24] M. I. Petkovic, A. M. Cvetkovic, G. T. Djordjevic, and G. K. Karagiannidis, "Partial relay selection with outdated channel state estimation in mixed RF/FSO systems," *J. Lightw. Technol.*, vol. 33, no. 13, pp. 2860–2867, Jul. 1, 2015.
[25] E. Soleimani-Nasab and M. Uysal, "Generalized performance analysis of mixed RF/FSO cooperative systems," *IEEE Trans. Wireless Commun.*, vol. 15, no. 1, pp. 714–727, Jan. 2016.
[26] N. Varshney and A. K. Jagannatham, "Cognitive decode-and-forward MIMO-RF/FSO cooperative relay networks," *IEEE Commun. Lett.*, vol. 21, no. 4, pp. 893–896, Apr. 2017.
[27] S. Sharma, A. S. Madhukumar, and R. Swaminathan, "Switching-based cooperative decode-and-forward relaying for hybrid FSO/RF networks," *IEEE/OSA J. Opt. Commun. Netw.*, vol. 11, no. 6, pp. 267–281, Jun. 2019.
[28] E. Balti and M. Guizani, "Mixed RF/FSO cooperative relaying systems with co-channel interference," *IEEE Trans. Commun.*, vol. 66, no. 9, pp. 4014–4027, Sep. 2018.
[29] N. H. Juel, A. S. M. Badrudduza, S. M. R. Islam, S. H. Islam, M. K. Kundu, I. S. Ansari, M. M. Mowla, and K.-S. Kwak, "Secrecy performance analysis of mixed α-μ and exponentiated Weibull RF-FSO cooperative relaying system," *IEEE Access*, vol. 9, pp. 72342–72356, 2021.
[30] X. Pan, H. Ran, G. Pan, Y. Xie, and J. Zhang, "On secrecy analysis of DF based dual hop mixed RF-FSO systems," *IEEE Access*, vol. 7, pp. 66725–66730, 2019.
[31] L. Yang, T. Liu, J. Chen, and M. Alouini, "Physical-layer security for mixed η-μ and $\mathcal{M}$-distribution dual-hop RF/FSO systems," *IEEE Trans. Veh. Technol.*, vol. 67, no. 12, pp. 12427–12431, Dec. 2018.
[32] A. Kumar and P. Garg, "Physical layer security for dual-hop FSO/RF system using generalized $\Gamma\Gamma/\eta - \mu$ fading channels," *Int. J. Commun. Syst.*, vol. 31, no. 3, pp. 1–12, 2018.
[33] S. H. Islam, A. S. M. Badrudduza, S. M. R. Islam, F. I. Shahid, I. S. Ansari, M. K. Kundu, and H. Yu, "Impact of correlation and pointing error on secure outage performance over arbitrary correlated nakagami-*m* and $\mathcal{M}$-turbulent fading mixed RF-FSO channel," *IEEE Photon. J.*, vol. 13, no. 2, pp. 1–17, Apr. 2021.
[34] H. Lei, Z. Dai, I. S. Ansari, K.-H. Park, G. Pan, and M.-S. Alouini, "On secrecy performance of mixed RF-FSO systems," *IEEE Photon. J.*, vol. 9, no. 4, pp. 1–14, Aug. 2017.
[35] Y. Ai, A. Mathur, H. Lei, M. Cheffena, and I. S. Ansari, "Secrecy enhancement of RF backhaul system with parallel FSO communication link," *Opt. Commun.*, vol. 475, Nov. 2020, Art. no. 126193.
[36] W. M. R. Shakir, "Physical layer security performance analysis of hybrid FSO/RF communication system," *IEEE Access*, vol. 9, pp. 18948–18961, 2021.
[37] K. O. Odeyemi, P. A. Owolawi, and O. O. Olakanmi, "Secrecy performance of cognitive underlay hybrid RF/FSO system under pointing errors and link blockage impairments," *Opt. Quantum Electron.*, vol. 52, no. 3, pp. 1–16, Mar. 2020.
[38] M. Kafafy, Y. Fahmy, M. Khairy, and M. Abdallah, "Secure backhauling over adaptive parallel mmWave/FSO link," in *Proc. IEEE Int. Conf. Commun. Workshops (ICC Workshops)*, Jun. 2020, pp. 1–6.
[39] S. Althunibat, R. Mesleh, and K. Qaraqe, "Secure index-modulation based hybrid free space optical and millimeter wave links," *IEEE Trans. Veh. Technol.*, vol. 69, no. 6, pp. 6325–6332, Jun. 2020.
[40] D. R. Pattanayak, V. K. Dwivedi, and V. Karwal, "On the physical layer security of hybrid RF-FSO system in presence of multiple eavesdroppers and receiver diversity," *Opt. Commun.*, vol. 477, Dec. 2020, Art. no. 126334.
[41] S. C. Tokgoz, S. Althunibat, S. Yarkan, and K. A. Qaraqe, "Physical layer security of hybrid FSO-mmWave communications in presence of correlated wiretap channels," in *Proc. IEEE Int. Conf. Commun. (ICC)*, Jun. 2021, pp. 1–7.
[42] S. C. Tokgoz, S. Althunibat, S. L. Miller, and K. A. Qaraqe, "On the secrecy capacity of hybrid FSO-mmWave links with correlated wiretap channels," *Opt. Commun.*, vol. 499, Nov. 2021, Art. no. 127252.
[43] A. K. Majumdar, "Free-space laser communication performance in the atmospheric channel," *J. Opt. Fiber Commun. Res.*, vol. 2, no. 4, pp. 345–396, Oct. 2005.
[44] L. C. Andrews, R. L. Phillips, and C. Y. Hopen, *Laser Beam Scintillation With Applications*, vol. 99, 2nd ed. Bellingham, WA, USA: SPIE Press, 2001.
[45] A. Jurado-Navas, J. M. Garrido-Balsells, J. F. Paris, A. Puerta-Notario, and J. Awrejcewicz, "A unifying statistical model for atmospheric optical scintillation," *Numer. Simulations Phys. Eng. Processes*, vol. 181, no. 8, pp. 181–205, 2011.
[46] A. Mathur, Y. Ai, M. R. Bhatnagar, M. Cheffena, and T. Ohtsuki, "On physical layer security of α-η-κ-μ fading channels," *IEEE Commun. Lett.*, vol. 22, no. 10, pp. 2168–2171, Oct. 2018.
[47] J. M. Moualeu, D. B. da Costa, W. Hamouda, U. S. Dias, and R. A. A. de Souza, "Physical layer security over α-κ-μ and α-η-μ fading channels," *IEEE Trans. Veh. Technol.*, vol. 68, no. 1, pp. 1025–1029, Jan. 2019.
[48] T. S. Rappaport, S. Sun, R. Mayzus, H. Zhao, Y. Azar, K. Wang, G. N. Wong, J. K. Schulz, M. Samimi, and F. Gutierrez, "Millimeter wave mobile communications for 5G cellular: It will work!" *IEEE Access*, vol. 1, pp. 335–349, 2013.
[49] A. I. Sulyman, A. T. Nassar, M. K. Samimi, G. R. MacCartney, Jr., T. S. Rappaport, and A. Alsanie, "Radio propagation path loss models for 5G cellular networks in the 28 GHz and 38 GHz millimeter-wave bands," *IEEE Commun. Mag.*, vol. 52, no. 9, pp. 78–86, Sep. 2014.
[50] S. Hur, S. Baek, B. Kim, Y. Chang, A. F. Molisch, T. S. Rappaport, K. Haneda, and J. Park, "Proposal on millimeter-wave channel modeling for 5G cellular system," *IEEE J. Sel. Topics Signal Process.*, vol. 10, no. 3, pp. 454–469, Apr. 2016.
[51] *3GPP Radio Access Network Working Group, Study on Channel Model for Frequencies From 0.5 to 100 GHz (Release 15)*, document 3GPP TR 38.901, TR ETSI TR 138 901 V14.3.0, 2018. [Online]. Available: https://www.etsi.org/deliver/etsi_tr/138900_138999/138901/14.03.00_60/tr_138901v140300p.pdf
[52] J. G. Andrews, T. Bai, M. N. Kulkarni, A. Alkhateeb, A. K. Gupta, and R. W. Heath, Jr., "Modeling and analyzing millimeter wave cellular systems," *IEEE Trans. Commun.*, vol. 65, no. 1, pp. 403–430, Jan. 2017.
[53] S. K. Yoo, S. L. Cotton, Y. J. Chun, W. G. Scanlon, and G. A. Conway, "Channel characteristics of dynamic off-body communications at 60 GHz under line-of-sight (LOS) and non-LOS conditions," *IEEE Antennas Wireless Propag. Lett.*, vol. 16, pp. 1553–1556, 2017.

[54] S. K. Yoo, S. L. Cotton, R. W. Heath, Jr., and Y. J. Chun, "Measurements of the 60 GHz UE to eNB channel for small cell deployments," *IEEE Wireless Commun. Lett.*, vol. 6, no. 2, pp. 178–181, Apr. 2017.
[55] M. K. Simon and M.-S. Alouini, *Digital Communication Over Fading Channels*, vol. 95, 2nd ed. Hoboken, NJ, USA: Wiley, 2005.
[56] U. Blahak, "Efficient approximation of the incomplete gamma function for use in cloud model applications," *Geosci. Model Develop.*, vol. 3, no. 2, p. 329, 2010.
[57] I. Gradshteyn and I. Ryzhik, *Table of Integrals, Series, and Products*, 7th ed. San Diego, CA, USA: Academic, 2014.
[58] A. Prudnikov, Y. A. Brychkov, and O. Marichev, *Integrals and Series, Elementary Functions*, vol. 1, 4th ed. New York, NY, USA: New York Gordon and Breach Science, 1992.
[59] M. Abramowitz, I. A. Stegun, and R. H. Romer, *Handbook of Mathematical Functions With Formulas, Graphs, and Mathematical Tables*. Annapolis, MD, USA: American Association of Physics Teachers, 1988.
[60] Z. Wang and G. B. Giannakis, "A simple and general parameterization quantifying performance in fading channels," *IEEE Trans. Commun.*, vol. 51, no. 8, pp. 1389–1398, Aug. 2003.
[61] I. I. Kim, B. McArthur, and E. J. Korevaar, "Comparison of laser beam propagation at 785 nm and 1550 nm in fog and haze for optical wireless communications," *Opt. Wireless Commun.*, vol. 4214, pp. 26–37, Feb. 2001.

SEZER C. TOKGOZ (Graduate Student Member, IEEE) was born in Istanbul, Turkey, in 1994. He received the B.S. degree in electrical and electronics engineering and the M.S. degree in electrical and telecommunications engineering from Istanbul Commerce University, in July 2017 and February 2019, respectively, and the M.S. degree in electrical and electronics engineering from Istanbul University, in January 2019. He is currently pursuing the Ph.D. degree in electrical engineering with the Department of Electrical and Computer Engineering, Texas A&M University, College Station, TX, USA. He holds a Ph.D. Merit Fellowship at the Department of Electrical and Computer Engineering, Texas A&M University. His current research interests include 5G and beyond radio access technologies, physical layer security, multi-carrier wireless systems, wireless channel measurement and modeling, and millimeter wave and optical communications.

SAUD ALTHUNIBAT (Senior Member, IEEE) received the Ph.D. degree in telecommunications from the University of Trento, Trento, Italy, in 2014. He is currently an Associate Professor with Al-Hussein Bin Talal University, Ma'an, Jordan. He has authored more than 100 scientific papers. His research interests include a wide range of wireless communication topics, such as index modulation, spectrum sharing, cognitive radio, wireless sensor networks, energy efficiency, and resource allocation. He is the General Co-Chair of BROADNETs 2018 Conference. He was a recipient of the Best Paper Award in IEEE CAMAD 2012, was selected as an Exemplary Reviewer for the IEEE COMMUNICATIONS LETTERS, in 2013, and was awarded Ali Mango for Distinguished Researcher, in 2021.

SCOTT L. MILLER (Fellow, IEEE) was born in Los Angeles, CA, USA, in 1963. He received the B.S., M.S., and Ph.D. degrees in electrical engineering from the University of California at San Diego (UCSD), in 1985, 1986, and 1988, respectively. He then joined the Department of Electrical and Computer Engineering, University of Florida, where he was an Assistant Professor, from 1988 to 1993, and an Associate Professor, from 1993 to 1998. In August 1998, he joined the Department of Electrical and Computer Engineering, Texas A&M University, where he is currently the Debbie and Dennis Segers '75 Professor and the Associate Dean for Graduate Programs at the Dwight Look College of Engineering. He has also held visiting positions at Motorola Inc., The University of Utah, and UCSD. He has taught courses at both the graduate and undergraduate level on such topics as linear circuits, signals and systems, engineering mathematics, digital and analog communications, probability and random processes, coding, information theory, spread spectrum, detection and estimation theory, wireless communications, signal processing, queuing theory, and communication networks. He has published over 75 refereed journal and conference papers on a variety of topics in the area of digital communication theory. His current research interests include the general area of wireless communications and signal processing. He is the Past Chair of the IEEE Communications Theory Technical Committee.

KHALID A. QARAQE (Senior Member, IEEE) was born in Bethlehem. He received the B.S. degree (Hons.) from the University of Technology, Bagdad, Iraq, in 1986, the M.S. degree from The University of Jordan, Amman, Jordan, in 1989, and the Ph.D. degree from Texas A&M University, College Station, TX, USA, in 1997, all in electrical engineering. From 1989 to 2004, he has held a variety positions in many companies and has over 12 years of experience in the telecommunication industry. He joined the Department of Electrical and Computer Engineering, Texas A&M University at Qatar, Qatar, in July 2004, where he is currently a Professor and the Managing Director of the Center for Remote Healthcare Technology, Qatar. He has worked on numerous projects and has experience in product development, design, deployments, testing, and integration. He has been awarded more than 20 research projects consisting of more than USD 13M from local industries in Qatar and the Qatar National Research Foundation (QNRF). He has published more than 131 journal articles in top IEEE journals, and has published and presented 250 papers at prestigious international conferences. He has 20 book chapters published, four books, three patents, and presented several tutorials and talks. His research interests include communication theory and its application to design and performance, analysis of cellular systems, and indoor communication systems. His particular research interests include mobile networks, broadband wireless access, cooperative networks, cognitive radio, diversity techniques, index modulation, visible light communication, FSO, tele-health, and noninvasive bio sensors.